Investigation Methods for Characterizing Nanoparticles in Concrete

Douglas Hendrix[1], Nabil Bassim[2], Kay Wille[3]

Synopsis There is significant potential for the use of nanoparticles in cementitious materials, especially in ultra-high performance concrete. These nanoparticles can further increase packing density, accelerate the pozzolanic reaction or can be used to induce new properties to the material, such as air purification or self-cleaning. Little is known about the interaction mechanisms between nanoparticles in cementitious materials, including their dispersion quality. The characterization of these nanoparticles can be challenging, especially when these nanoparticles interact with cementitious materials and their reaction products during hydration. Thorough characterization of the nanoparticle system is essential to understand how to optimize mixing constituents, procedures, and parameters.

This study explores the feasibility and potential use of several characterization methods for investigating colloidal nanosilica in a concrete environment. These techniques include dynamic light scattering, zeta potential, atomic force microscopy, scanning electron microscopy, cryogenic SEM, and focused ion beam microscopy. These methods allow for characterization of nanoparticles, nanoparticles interacting with pore solution that represents a concrete environment, nanoparticles interacting with polymers used as superplasticizers, and nanoparticles interacting with a cementitious material. These tools allow for studies on the nano-length scale at short times to observe and measure parameters such as particle size distribution, polydispersity index, and zeta potential.

Keywords: characterization, nanoparticles, cementitious material, concrete, dispersion, size distribution, dynamic light scattering

Douglas Hendrix

[1]Ph.D Student, Department of Materials Science and Engineering, University of Connecticut

Doug Hendrix is a PhD candidate in the Materials Science and Engineering program at the University of Connecticut where he received his Bachelor's degree as well. His research is focused on material characterization and development of ultra-high performance concrete advised by Dr. Kay Wille. In fall of 2018 he won the IMS Graduate Student Presentation Competition.

Kay Wille

[3]Associate Professor, Civil and Environmental Engineering, University of Connecticut

Dr. Wille graduated with a Ph.D. degree in Civil Engineering atfrom the University of Leipzig, Germany in 2008. Afterw postdoctoral research at the University of Michigan Dr. Wille accepted a faculty position at the University of Connecticut in 2010. Dr. Wille serves in several committees related to his research interest, such as ACI 239, ACI 241 and ACI 544. In 2015 he received the NSF CAREER award..

Nabil Bassim

[2]Associate Professor, Department of Materials Science and Engineering, McMaster University, ON, Canada,

Dr. Bassim graduated with a Ph.D. degree from the University of Florida in Materials Science and Engineering in 2002. He worked as a Materials Research Engineer at the U.S. Naval Research Laboratory in the high-resolution characterization of materials using ions and electrons. Bassim has since moved to McMaster University, where he continues to develop tomography techniques for mesoscale solids and currently acts as the Scientific Director of the Canadian Centre for Electron Microscopy.

INTRODUCTION

There is an ever-growing desire to improve material properties such as strength, toughness, ductility, and density. These are driven by a variety of factors including cost reduction and environmental concerns. The concrete industry is no exception to this. The strength of concrete has increased dramatically over the past decade, resulting in a type of concrete known as ultra-high performance concrete (UHPC).[1–3] UHPC is defined as having a minimum compressive strength of 150 MPa (22,000 psi).[4] With the use of fibers, UHPC can possess high strength and high ductility simultaneously.[5–7] UHPC achieves these properties through increased particle packing and increased pozzolanic reactions.[8–12]

The desire to further push the limits of UHPC has led to the use of nanoparticles in the cementitious matrix. It is hypothesized that nano-sized particles can further enhance the particle packing and contribute to the pozzolanic reaction.[13–16] Implementation of nanoparticles in cementitious materials has proved to be challenging due to several factors including their high surface area to volume ratio, resulting in large surface energies.[17–19] These surface energies often result in agglomeration of nanoparticles, as their attractive forces are much greater than their repulsive forces. It is a challenge across many disciplines to achieve a uniform and stable dispersion of nanoparticles.[20–23] This is also the case in cementitious materials which have a high pH and many different ions dynamically reacting in the system.[24–26]

The characterization of nanoparticles is critical to understanding how they react in a cementitious material. There are many methods available for the study of nanoparticles, often found in the materials science, chemistry, and electronics disciplines. A further challenge is studying these particles in a cement-based material. Since concrete is one of the most complex materials systems to study, introducing highly reactive nanoparticles into the system only complicates matters.[27,28]

Researchers have attempted to study nanoparticles, the effects of superplasticizers, and how these affect concrete properties.[29–32] There are a variety of techniques that have been used to study nanoparticles, such as forms of electron microscopy, laser light scattering, scanning probe microscopy, x-ray microscopy, Fourier-transform infrared spectroscopy (FTIR), thermogravimetric analysis (TGA), differential scanning calorimetry (DSC), nuclear magnetic resonance (NMR), and many more.[33–42] There has been a desire to bridge the gap between macroscopic properties of concrete in the civil engineering field down to the nano-scale materials properties and interactions in the materials science arena.

This study compares several characterization techniques that are useful in the study of nanoparticles, nanoparticles interacting with superplasticizers, and nanoparticles in cement-based systems. Techniques investigated were dynamic light scattering (DLS), zeta potential (ζp), scanning electron microscopy (SEM), cryogenic SEM (cryoSEM), focused ion beam (FIB), and atomic force microscopy (AFM).

MATERIALS AND METHODS

Nanoparticles

The nanoparticles used in this study were colloidal silica. Colloidal silica was chosen over powdered silica because colloidal silica is already uniformly dispersed in solution. Four different sols of varying average diameters in different stabilizing ions were used: 5 nm (1.97×10^{-7} in) with ammonium (NS-5), 20 nm (7.87×10^{-7} in) with no stabilizing ion (NS-20a), 20 nm with sodium (NS-20b), and 75 nm (2.95×10^{-6} in) with sodium (NS-75). A full list of materials properties as provided by the manufacturer are in **Error! Reference source not found.**.

Table 1— Properties of nanosilica sols. 5 nm ≈ 1.97×10^{-7} in. 100 $m^2/g \approx 7.03\times10^7$ in^2/lb. 10 cP ≈ 5.60×10^{-4} lb/in s

	NS-5	NS-20a	NS-20b	NS-75
Particle Size (nm)	5	20	20	75
Surface area (m^2/g)	600	150	150	40
% SiO_2	15	34	50	40
pH	9.0	2.8	9.0	8.4
Specific Gravity	1.09	1.23	1.39	1.29
Viscosity (cP)	< 10	< 10	55	10
Stabilizing Ion	Ammonium	--	Sodium	Sodium
% Na_2O	0.02	0.04	0.40	0.30

Dynamic Light Scattering

DLS was used extensively for the characterization of the NS sols. DLS was used to determine the particle size distribution (PSD) of the sols under various conditions. DLS measures the changing intensity of scattered light from particles under Brownian motion in a suspension. By analyzing this data, a variety of measurements can be made including PSD. DLS measurements were performed on a commercially available system using disposable polystyrene cuvettes at room temperature (25°C, 77°F). Samples were prepared within one hour of measurement and were equilibrated at this temperature for 30 seconds before measurement. The dispersant (water) properties were set to a viscosity of 0.8872 cP (4.953×10^{-5} lbs/in s) and a refractive index of 1.330. The material absorption coefficient was set to 0.001 and their refractive index to 1.50. The angle of detection was 173°. Three measurements were performed for each sample at 11 runs per measurement, 10 seconds per run. All data reported are the mean of the corresponding three measurements.

DLS allows for in situ measurements of nanoparticles in a variety of suspensions. The effects of pH, ionic concentration, and others can be quickly quantified using DLS. Sample preparation requires no specialized equipment and small volumes of sample are sufficient. However, since DLS requires samples to be in a suspension, the chemistry must represent the system the nanoparticles will be introduced to. The equipment has restrictions based on particle size and cannot analyze particles larger than about 1 μm (3.94×10^{-5} in). The particle size distribution also cannot be polydisperse.

Zeta Potential

ζp was used as an additional method to quantify the stability of the sol. ζp is a measure of the electrostatic potential between particles. A greater magnitude of ζp indicates a better stability, compared to a lower value which could indicate partial or no stability. Generally, ζp greater than 30 mV indicates good stability while values less than this can lead to destabilization and agglomeration. ζp was done using a dip cell accessory in the same DLS system. ζp was performed immediately after DLS in the same sample cuvette. Four measurements were performed for each sample at 30 runs per measurement. The remaining parameters were kept consistent with those from DLS.

Samples for both DLS and ζp were prepared using the NS sols, DI water, aqueous 0.1M potassium hydroxide (KOH), calcium nitrate ($Ca(NO_3)_2{\cdot}4H_2O$), and a synthetic pore solution (PS) as outlined by Schrofl et. al (9.72 g (0.34 oz) $Ca(NO_3)_2{\cdot}4H_2O$ dissolved in 148.5 g (5.24 oz) of 0.1 mol/L aqueous KOH solution).[43] A variety of parameters were explored including varying the solids concentration, pH, and amounts of PS. The PS was filtered to 0.1μm (3.94×10^{-6} in) before use.

ζp has all of the same advantages and disadvantages as DLS. In addition, ζp can be easily influenced by the pH of a solution. For most nanoparticle systems, ζp accurately predicts stability. However, this can break down in a silica system at low pH.

Electron Microscopy

Two methods were used to visualize nanoparticles in a cementitious material: cryoSEM and FIB sectioning with SEM imaging. For cryoSEM, samples were prepared by plunging into a liquid nitrogen slush, fractured, etched, and sputter coated with Au/Pt. NS sols, a superplasticizer (SP), and a cement paste containing white Portland cement (Type I, ASTM C150) and NS-75 were imaged. The cement paste was mixed in an acoustic mixer at an intensity of 50% for a total mixing time of 300 seconds. The time between initial hydration and freezing was 1 hour.

Dual-beam FIB & SEM were used to visualize the microstructure in three dimensions. The sample contained Al_2O_3 nanoparticles (similar in size to the NS sols) in a high performance concrete mix. A Plasma FIB equipped with a xenon source was used to perform serial sectioning tomography of 150 um x 100 um x 40 um (5.91×10^{-3} in x 3.93×10^{-3} in x 1.57×10^{-3} in) volume with a slice depth of 50 nm (1.97×10^{-6} in) . Images were acquired in backscatter mode at 2 keV. The voxel resolution was 50 nm x 50 nm x 50 nm (1.97×10^{-6} in x 1.97×10^{-6} in x 1.97×10^{-6} in).

Electron microscopy is a versatile technique to study a variety of materials. It offers imaging on a large length scale, with an ultimate lateral resolution of about 1 nm (3.94×10^{-8} in. It has a large depth of field and accepts a variety of sample sizes and geometries. However, most electron microscopy techniques require the sample to be electrically conductive. To mitigate this, samples can be coated with a thin conductive layer. Electron microscopy is

commonly done in a high vacuum so samples must be free of moisture. Organic materials are also susceptible to damage from the electron beam.

Atomic Force Microscopy

AFM was used to image the NS sols, NS interacting with SP, and a UHPC sample. A silicon probe with a 160 μm (6.30×10^{-3} in) long cantilever was used with a resonance frequency of 300 kHz and a spring constant of 26 N/m (230 in/lbs). All imaging was done in air in intermittent contact mode. NS samples drop cast on a glass slide. The UHPC sample was lightly ground with 800 grit SiC paper for 90 seconds. Several AFM modes can be used to characterize nanoparticles, especially in cement-based systems. For example, Ferrari et al measured the interaction forces between nanoparticles and pore solution.[44] Others have studied the hydration structure and morphology containing nanosized particles.[45] The authors plan on studying the forces between nanoparticles and various superplasticizers using AFM to further understand the dispersion mechanisms.

AFM can characterize a wide variety of materials with excellent lateral and spatial resolution. In addition to topography, AFM can measure may other properties such as electrical conductivity, magnetic domains, and biological properties. However, AFM generally requires small sample sizes. Samples also must be relatively smooth, often less than 10 μm of surface roughness.

RESULTS AND DISCUSSION

Nanoparticle Characterization

In order to characterize nanoparticles in a cement-based system, it was necessary to first characterize the nanoparticles alone. This was accomplished by using DLS, SEM, and AFM. This proved to be a quick and simple method to determine particle shape and size. Shown in Figure 1, NS-75 was imaged with SEM and AFM. It is apparent that these particles are spherical in shape with particle sizes between 65 nm and 90 nm (2.56×10^{-6} in and 3.54×10^{-6} in). These two methods are relatively straightforward to image nanoparticles of this size. However, imaging particles of smaller sizes (< 20 nm (7.87×10^{-7} in)) becomes more difficult. In AFM, resolution is ultimately limited by the probe geometry and tip radius. It becomes more difficult to resolve individual particles on this length scale. SEM is also limited in its capabilities for imaging small nanoparticles. Resolution is limited by the spot size of the electron beam and the interaction volume of the electrons in the material. Some of these challenges with imaging particles less than 20 nm (7.87×10^{-7} in) can be overcome with more advanced equipment and technique, but for intermediate sizes, these two methods are sufficient.

During sample preparation for standard use cases of SEM and AFM, it proved to be difficult to isolate individual nanoparticles. As apparent in Figure 1, the nanoparticles are agglomerated and very few isolated particles are observed. This observation is due to the effects of drying in ambient conditions on the NS sols. The removal of water eliminates the electrostatic repulsion between particles. SEM and AFM were also used to qualitatively observe the interaction of nanoparticles and a superplasticizer. Both techniques produced qualitatively similar results, where the nanoparticles formed long chains and rings as a result of the interaction with the superplasticizer. CryoSEM can mitigate drying effects, as the samples are rapidly frozen, preserving the microstructure and minimizing sample artifacts. Then the ice is sublimed to reveal the microstructure. CryoSEM was used to visualize the nanoparticles and the interaction between nanoparticles and superplasticizer, depicted in Figure 2. Again, qualitatively similar images were observed and compared to SEM and AFM.

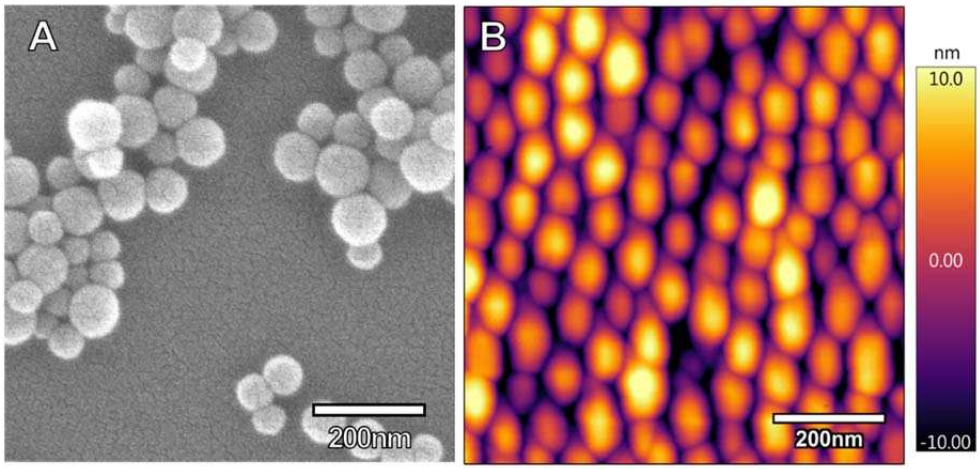

Figure 1 — Images of NS-75 with A) SEM and B) AFM showing their spherical morphology and their tendency to agglomerate. 200 nm ≈ 7.87×10^{-6} in.

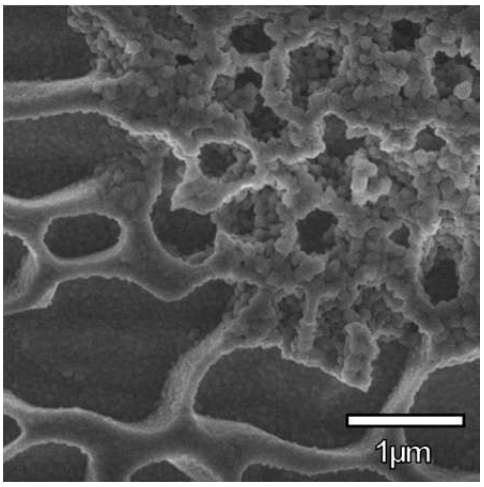

Figure 2 — cryoSEM image of agglomeration of NS-75 with a superplasticizer. The structure of the polymer is visible on the left while the nanoparticles are in the upper right. 1 µm ≈ 3.94×10^{-5} in.

To quantitatively study the PSD and stability of the NS sols, DLS and ζp were used. DLS can be sensitive to several parameters such as sample concentration, particle size, and sample temperature. For these reasons, a range of sample concentrations were employed, from 0.2% solid through the solid concentration of the as received state.

As reported by the authors elsewhere (under submission), the ideal concentration for the NS sols was 2% solid.

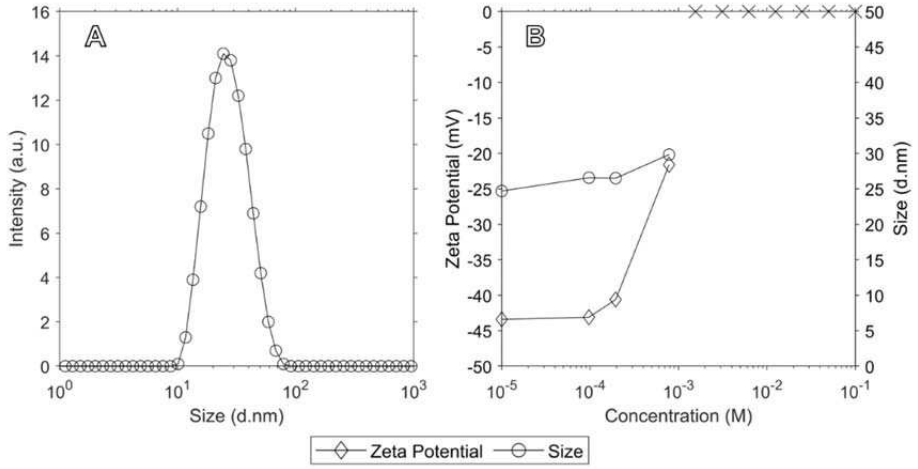

Figure **3**a is the PSD for NS-20b at 2% solid. This is an example of a monomodal distribution of particles, with the z-average size reported as 24.7 nm ± 0.2 nm (9.72×10^{-7} in ± 7.87×10^{-9} in). From DLS, a discrete distribution of sizes can be obtained. This is important for understanding how the particles might react with cement-based systems because factors such as particle packing can be important. A complimentary technique to DLS, ζp, was used to determine the stability of the NS sols. At 2% solid, the ζp was -43.4 mV ± 0.4 mV. This indicates a stable sol as the magnitude of the electrostatic potential is sufficient to keep particles from agglomerating.

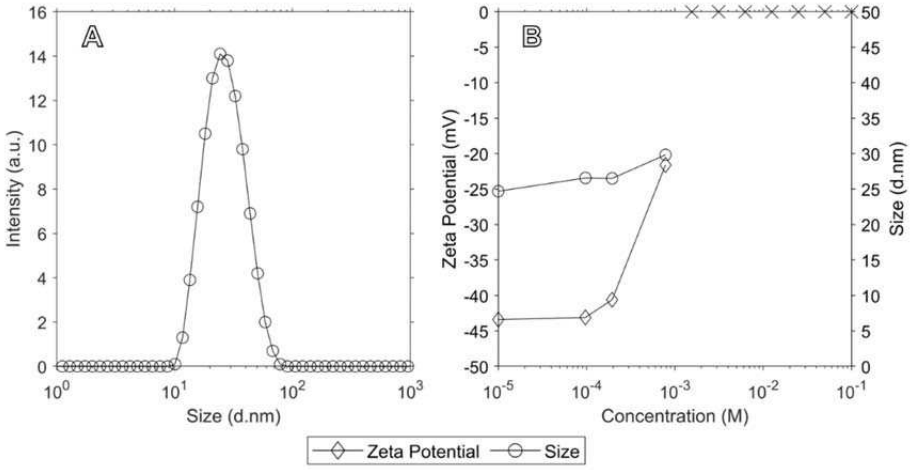

Figure 3 — Plot of a) PSD of NS-20b at 2% solid in DI water and B) average size and zeta potential as a function of the concentration of synthetic PS. X's indicate agglomeration and complete instability. 10 nm ≈ 3.94×10^{-7} in.

Nanoparticles in Cementitious Material Characterization

A major challenge of current concrete research is the ability to observe nanoparticles in a cement-based system. In efforts to understand what happens to nanoparticles in concrete, experiments were conducted to best simulate the concrete environment. Using DLS and ζp, the interactions of nanoparticles could be studied. Using this methodology, samples were able to be rapidly created and tested with less sample volume and waste. Synthetic pore solution was used to represent the concrete environment, comprised of KOH and $Ca(NO_3)_2$. The individual components were added to NS sols in varying concentrations to understand how certain ions reacted with NS. Then PS was added to NS sols, again in varying concentrations. The PSD and ζp were measured throughout. As PS increased in concentration, up to its maximum concentration, the average particle size increased and the ζp

decreased, indicating that with increasing ionic strength and pH, the sols become less stable and begin to

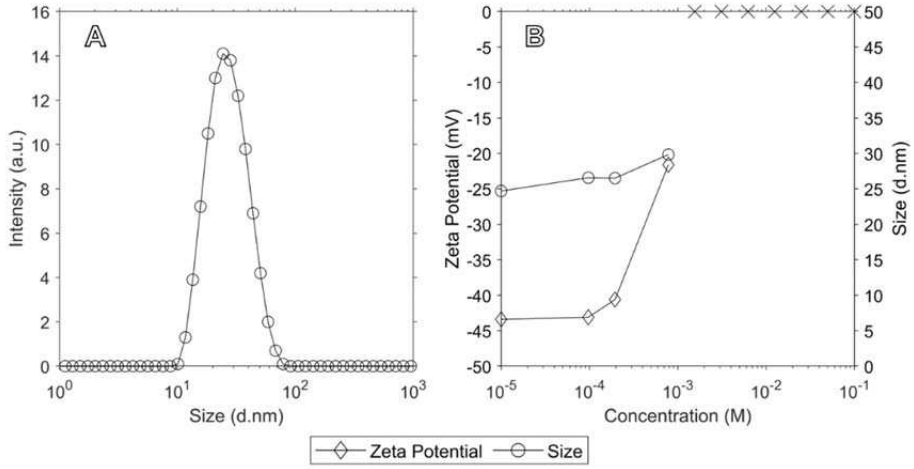

agglomerate.

Figure **3**b is a plot of ζp and average particle size as a function of PS concentration. At a concentration higher than 7.81×10^{-4} M, the NS agglomerates rapidly and becomes unstable, as indicated byX's. It is hypothesized that this same effect will occur when the NS is put into a concrete mix, which would lead to significant agglomeration and decrease the effects of particle packing.

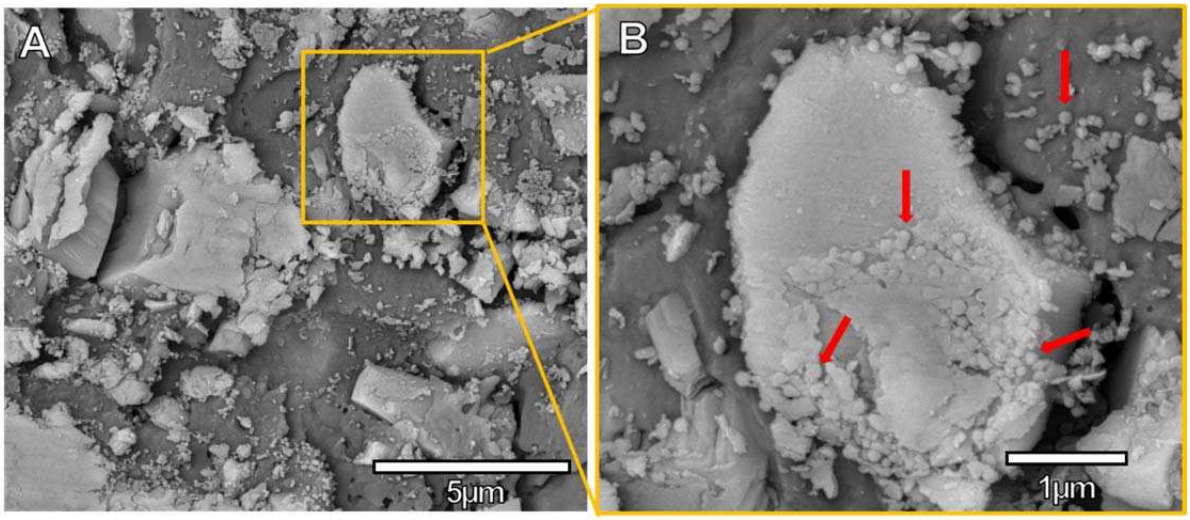

Figure 4 — cryoSEM images of a cement paste sample containing NS-75. The inset (B) shows individual nanoparticles on a cement grain, highlighted by red arrows. 1 μm ≈ 3.94×10^{-5} in.

It is important to observe the nanoparticles in a cement-based system to correlate data from the synthetic PS experiments. The concrete microstructure was observed using three techniques: cryoSEM, FIB/SEM sectioning, and AFM.

CryoSEM has the unique ability to stop hydration at a very specific time to observe time-dependent effects. Figure 4 is an image of a cement and NS sample at a time of 1 hour after initial hydration. The sample components were kept minimal in order to best observe the nanoparticles. The time of hydration was also kept short because NS can be consumed by the hydration products of cement. From the figure, it is apparent there is a range of cement particle sizes, from about 2 to 10 μm (7.87×10^{-5} in to 3.94×10^{-4} in). In Figure 4b, NS particles are observed on a cement grain and in the aqueous matrix surrounding the cement, highlighted by red arrows. In these images, the darker background typically indicates ice that had not been sublimated. Most of the particles are agglomerated, which confirms the findings from DLS. Nanoparticles were also not observed everywhere, indicating further

dispersion issues. CryoSEM will be a powerful tool to observe the evolving microstructure and to study the effect of nanoparticles on a very small length and time scale.

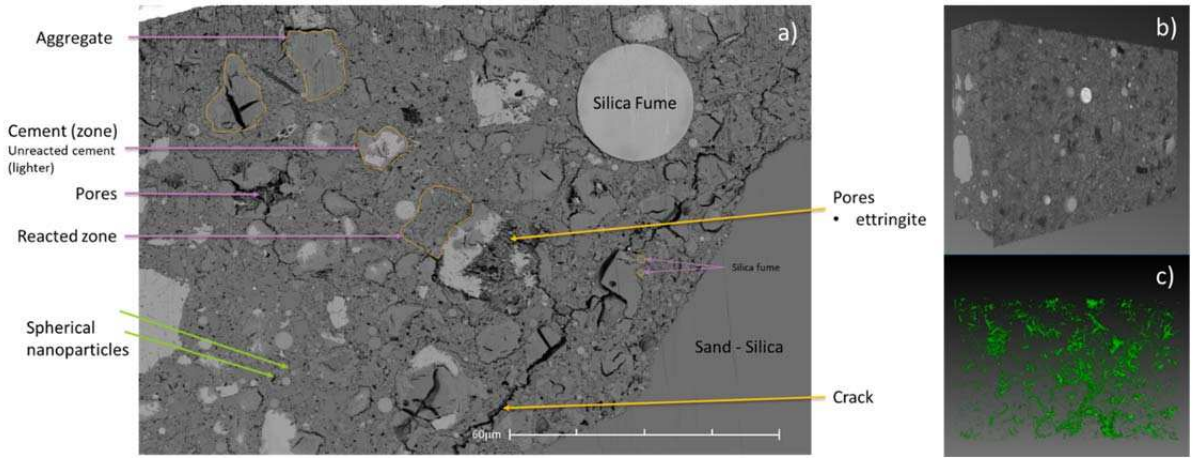

Figure 5 — a) A BSE SEM image from a FIB serial section tomogram, b) the 3d volumetric reconstruction of the data and c) threshold segmentation of the pore/crack network within the volume. 60 µm ≈ 2.36×10^{-3} in.

In addition to observing the microstructure at short times, it is also important to understand the developed, mature microstructure. As stated earlier, this can be difficult with traditional optical and electron microscopy. These two methods only allow for surface imaging and may not be representative of the entire structure. Through the use of FIB serial sectioning, tomographic data was collected to understand the microstructure in three dimensions. Figure 5a is an SEM image of one slice from the dataset. There are many different phases, components, and structures of this concrete sample containing Al_2O_3 nanoparticles, silica fume, and sand. The Al_2O_3 nanoparticles are of similar size to the nanosilica used. The authors' best efforts to identify the phases are highlighted on the figure. Since imaging occurs in a larger volume, this data can be reconstructed into a 3D volume, demonstrated in Figure 5b. This helps to visualize the microstructure as features are no longer limited to two-dimensional viewing. One example is the use of thresholding to find the pores and cracks within this volume, show in Figure 5c. The distribution of distinct phases can also be quantified and visualized in the 3D volume. FIB can polish the sample surface with minimal mechanical damage, enabling the maximum contrast from BSE SEM imaging. Traditional polishing techniques can be destructive, difficult to implement, and time consuming. FIB can also be used for higher-resolution transmission electron microscopy (TEM) sample preparation to further study the nanoparticle-matrix interaction.

AFM of concrete surfaces is a technique that is not often used because AFM requires samples to be relatively smooth. However, AFM has a large potential for characterizing the microstructure of concrete. Figure 6 is a topographic image of a UHPC surface. There are scratch marks from mechanical polishing clearly visible in the image. This is an example of how polishing techniques can be destructive and difficult. From this simple topographic image, it is apparent that there are many interesting structures visible. There are small voids and pits in the material of varying shapes and sizes. There are also regions of small protruding features. Further work to understand the microstructure is ongoing. From the various data channels that intermittent contact mode can provide, such as phase, material contrast can be observed between different phases of the concrete material. This high-resolution technique can allow for characterization on very small length scales with nanometer vertical resolution.

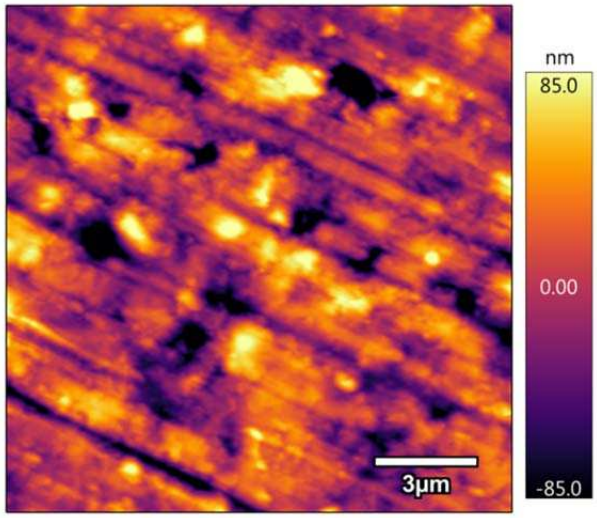

Figure 6 — Topographic AFM image of UHPC. 3 µm ≈ 1.18×10^{-4} in. 85 nm ≈ 3.35×10^{-6} in.

CONCLUSION

In this study, several characterization techniques were studied for their efficacy in studying nanoparticles in cementitious materials. These techniques can be applied to a wide range of materials and have the ability to observe different length and time scales which are important to further understand particle behavior in cement-based systems. In order to further increase concrete strength, durability, and other desirable mechanical and functional properties, a larger effort must be placed on the materials science of this complex materials system.
In conclusion:

- SEM and AFM are excellent tools for quickly visualizing the shape and size of nanoparticles of similar diameter to those used in this study.
- DLS and ζp are simple tools to identify NS sols and polymers that might work well in a concrete mix. It allows for rapid sample creation and testing that can provide a wealth of information regarding the behavior of particles in a certain environment. A synthetic PS was used to simulate the concrete environment to observe the stability and agglomeration of NS.
- CryoSEM is a versatile tool for exploring NS sols, NS sols interacting with polymers, and a variety of cementitious materials. It has the distinct ability to image the microstructure at discrete hydration times. Samples can contain water and do not have artifacts from drying. Agglomerated NS particles were clearly observed on cement grains.
- FIB and SEM are a powerful combination of methods to explore concrete microstructure in three dimensions with high spatial resolution. The ability to view a tomographic dataset provides a greater understanding of a material and can provide insight about microstructures. A concrete sample containing Al_2O_3 particles was imaged and the nanoparticles were clearly visible in the microstructure.

ACKNOWLEDGEMENT

This research has been supported by the National Science Foundation CMMI Grant 1454574, CAREER: Understanding Behavior and Properties of Nano-Sized Particles in Cement-Based Materials.

References

1. Rossi, P., Arca, A., Parant, E. & Fakhri, P. Bending and compressive behaviours of a new cement composite. *Cem. Concr. Res.* **35**, 27–33 (2005).

2. Richard, P. & Cheyrezy, M. Composition of reactive powder concretes. *Cem. Concr. Res.* **25**, 1501–1511 (1995).

3. Aïtcin, P.-C. Cements of yesterday and today - concrete of tomorrow. *Cem. Concr. Res.* **30**, 1349–1359 (2000).

4. Wille, K., Naaman, A. E. & Parra-Montesinos, G. J. Ultra-High Performance Concrete with Compressive Strength Exceeding 150 MPa (22 ksi): A Simpler Way. *ACI Mater. J.* **108**, (2011).

5. Wille, K. & Naaman, A. E. Effect of ultra-high-performance concrete on pullout behavior of high-strength brass-coated straight steel fibers. *ACI Mater. J.* **110**, 451 (2013).

6. Pansuk, W., Sato, H., Sato, Y. & Shionaga, R. Tensile behaviors and fiber orientation of UHPC. in *Proceedings of second international symposium on ultra high performance concrete, Kassel, Germany* 161–168 (2008).

7. Wu, Z., Shi, C., He, W. & Wu, L. Effects of steel fiber content and shape on mechanical properties of ultra high performance concrete. *Constr. Build. Mater.* **103**, 8–14 (2016).

8. de Larrard, F. & Sedran, T. Optimization of ultra-high-performance concrete by the use of a packing model. *Cem. Concr. Res.* **24**, 997–1009 (1994).

9. Scrivener, K. L. & Kirkpatrick, R. J. Innovation in use and research on cementitious material. *Cem. Concr. Res.* **38**, 128–136 (2008).

10. Pfeifer, C., Moeser, B., Weber, C. & Stark, J. Investigations of the pozzolanic reaction of silica fume in ultra high performance concrete (UHPC). in *International RILEM Conference on Material Science* 287–298 (RILEM Publications SARL, 2010).

11. Tagnit-Hamou, N. A. S. and A. Using Particle Packing and Statistical Approach to Optimize Eco-Efficient Ultra-High-Performance Concrete. *Mater. J.* **114**,

12. Yu, R., Spiesz, P. & Brouwers, H. J. H. Mix design and properties assessment of Ultra-High Performance Fibre Reinforced Concrete (UHPFRC). *Cem. Concr. Res.* **56**, 29–39 (2014).

13. Collepardi, M., Collepardi, S., Skarp, U. & Troli, R. Optimization of silica fume, fly ash and amorphous nano-silica in superplasticized high-performance concretes. in *Proceedings of 8th CANMET/ACI International Conference on Fly Ash, Silica Fume, Slag and Natural Pozzolans in Concrete, SP-221, Las Vegas, USA* 495–506 (Citeseer, 2004).

14. Björnström, J., Martinelli, A., Matic, A., Börjesson, L. & Panas, I. Accelerating effects of colloidal nano-silica for beneficial calcium–silicate–hydrate formation in cement. *Chem. Phys. Lett.* **392**, 242–248 (2004).

15. Kawashima, S., Hou, P., Corr, D. J. & Shah, S. P. Modification of cement-based materials with nanoparticles. *Cem. Concr. Compos.* **36**, 8–15 (2013).

16. Aggarwal, P., Singh, R. P. & Aggarwal, Y. Use of nano-silica in cement based materials—A review. *Cogent Eng.* **2**, 1078018 (2015).

17. Bagheri, A., Parhizkar, T., Madani, H. & Raisghasemi, A. M. The influence of different preparation methods on the aggregation status of pyrogenic nanosilicas used in concrete. *Mater. Struct.* **46**, 135–143 (2013).

18. Khaloo, A., Mobini, M. H. & Hosseini, P. Influence of different types of nano-SiO2 particles on properties of high-performance concrete. *Constr. Build. Mater.* **113**, 188–201 (2016).

19. Qing, Y., Zenan, Z., Deyu, K. & Rongshen, C. Influence of nano-SiO2 addition on properties of hardened cement paste as compared with silica fume. *Constr. Build. Mater.* **21**, 539–545 (2007).

20. Hayrapetyan, S. S. & Khachatryan, H. G. Control of the growth processes of the silica sols colloidal particles. *Microporous mesoporous Mater.* **78**, 151–157 (2005).

21. Kamiya, H. & Iijima, M. Surface modification and characterization for dispersion stability of inorganic nanometer-scaled particles in liquid media. *Sci. Technol. Adv. Mater.* **11**, 44304 (2010).

22. Lazzara, G. & Milioto, S. Dispersions of nanosilica in biocompatible copolymers. *Polym. Degrad. Stab.* **95**, 610–617 (2010).

23. Kang, S.; Hong, S. Il; Choe, C. R.; Park, M.; Rim, S.; Kim, J. Preparation and characterization of epoxy composites filled with functionalized nanosilica particles obtained via sol–gel process. *Polymer (Guildf).* **42**, 879–887 (2001).

24. Oertel, T., Hutter, F., Helbig, U. & Sextl, G. Amorphous silica in ultra-high performance concrete: First hour of hydration. *Cem. Concr. Res.* **58**, 131–142 (2014).

25. Bullard, J. W.; Jennings, H. M.; Livingston, R. A.; Nonat, A.; Scherer, G. W.; Schweitzer, J. S.; Scrivener, K. L.; Thomas, J. J. Mechanisms of cement hydration. *Cem. Concr. Res.* **41**, 1208–1223 (2011).

26. Plank, J., Schroefl, C., Gruber, M., Lesti, M. & Sieber, R. Effectiveness of polycarboxylate superplasticizers in ultra-high strength concrete: the importance of PCE compatibility with silica fume. *J. Adv. Concr. Technol.* **7**, 5–12 (2009).

27. Jennings, H. M.; Bullard, J. W.; Thomas, J. J.; Andrade, J. E.; Chen, J. J.; Scherer, G. W. Characterization and modeling of pores and surfaces in cement paste. *J. Adv. Concr. Technol.* **6**, 5–29 (2008).

28. Jalilvand, S. & Shahsavari, R. Molecular Mechanistic Origin of Nanoscale Contact, Friction, and Scratch in Complex Particulate Systems. *ACS Appl. Mater. Interfaces* **7**, 3362–3372 (2015).

29. Kontoleontos, F., Tsakiridis, P. E., Marinos, A., Kaloidas, V. & Katsioti, M. Influence of colloidal nanosilica on ultrafine cement hydration: Physicochemical and microstructural characterization. *Constr. Build. Mater.* **35**, 347–360 (2012).

30. Madani, H., Bagheri, A. & Parhizkar, T. The pozzolanic reactivity of monodispersed nanosilica hydrosols and their influence on the hydration characteristics of Portland cement. *Cem. Concr. Res.* **42**, 1563–1570 (2012).

31. Land, G. & Stephan, D. The influence of nano-silica on the hydration of ordinary Portland cement. *J. Mater. Sci.* **47**, 1011–1017 (2012).

32. Singh, L. P., Karade, S. R., Bhattacharyya, S. K., Yousuf, M. M. & Ahalawat, S. Beneficial role of nanosilica in cement based materials–A review. *Constr. Build. Mater.* **47**, 1069–1077 (2013).

33. Zhang, M. Q., Rong, M. Z., Zhang, H. B. & Friedrich, K. Mechanical properties of low nano-silica filled high density polyethylene composites. *Polym. Eng. Sci.* **43**, 490–500 (2004).

34. Su, C., Li, J., Geng, H., Wang, Q. & Chen, Q. Fabrication of an optically transparent super-hydrophobic surface via embedding nano-silica. *Appl. Surf. Sci.* **253**, 2633–2636 (2006).

35. Amiri, B., Bahari, A., Nik, A. S., Nik, A. S. & Movahedi, N. S. Use of AFM technique to study the nano-silica effects in concrete mixture. *Indian J. Sci. Technol.* **5**, 2055–2059 (2012).

36. Li, X., Cao, Z., Zhang, Z. & Dang, H. Surface-modification in situ of nano-SiO2 and its structure and tribological properties. *Appl. Surf. Sci.* **252**, 7856–7861 (2006).

37. Davis, K. E., Russel, W. B. & Glantschnig, W. J. Settling suspensions of colloidal silica: observations and X-ray measurements. *J. Chem. Soc. Faraday Trans.* **87**, 411–424 (1991).

38. Luo, T.; Huang, P.; Gao, G.; Shen, G.; Fu, S.; Cui, D.; Zhou, C.; Ren, Q. Mesoporous silica-coated gold nanorods with embedded indocyanine green for dual mode X-ray CT and NIR fluorescence imaging. *Opt. Express* **19**, 17030–17039 (2011).

39. Ikeda, Y., Katoh, A., Shimanuki, J. & Kohjiya, S. Nano-Structural Observation of in situ Silica in Natural Rubber Matrix by Three Dimensional Transmission Electron Microscopy. *Macromol. Rapid Commun.* **25**, 1186–1190 (2004).

40. Chen, X., Wu, L., Zhou, S. & You, B. In situ polymerization and characterization of polyester-based polyurethane/nano-silica composites. *Polym. Int.* **52**, 993–998 (2003).

41. Aly, M.; Hashmi, M. S. J.; Olabi, A. G.; Messeiry, M.; Abadir, E. F.; Hussain, A. I. Effect of colloidal nano-silica on the mechanical and physical behaviour of waste-glass cement mortar. *Mater. Des.* **33**, 127–135 (2012).

42. Che, J.; Xiao, Y.; Wang, X.; Pan, A.; Yuan, W.; Wu, X. Grafting polymerization of polyacetal onto nano-silica surface via bridging isocyanate. *Surf. Coatings Technol.* **201**, 4578–4584 (2007).

43. Schröfl, C., Gruber, M. & Plank, J. Preferential adsorption of polycarboxylate superplasticizers on cement and silica fume in ultra-high performance concrete (UHPC). *Cem. Concr. Res.* **42**, 1401–1408 (2012).

44. Ferrari, L., Kaufmann, J., Winnefeld, F. & Plank, J. Interaction of cement model systems with superplasticizers investigated by atomic force microscopy, zeta potential, and adsorption measurements. *J. Colloid Interface Sci.* **347**, 15–24 (2010).

45. Peled, A. & Weiss, J. Hydrated cement paste constituents observed with Atomic Force and Lateral Force Microscopy. *Constr. Build. Mater.* **25**, 4299–4302 (2011).